Published in final edited form as:
Exp Neurol. 2015 February ; 264: 43–54. doi:10.1016/j.expneurol.2014.12.001.

Spreading Depression Transiently Disrupts Myelin via Interferon-gamma Signaling

Aya D. Pusic[a,b], **Heidi M. Mitchell**[a], **Phillip E. Kunkler**[a], **Neal Klauer**[a], and **Richard P. Kraig**[a,b,*]

Aya D. Pusic: aya.pusic@gmail.com; Heidi M. Mitchell: heidi.marie.mitchell@gmail.com; Phillip E. Kunkler: golgi61@aol.com; Neal Klauer: nealklauer12@gmail.com

[a]Department of Neurology, The University of Chicago Medical Center, 5841 South Maryland Avenue, Chicago, IL 60637-1470, USA

[b]The Committee on Neurobiology, The University of Chicago Medical Center, 5841 South Maryland Avenue, Chicago, IL 60637-1470, USA

Abstract

Multiple sclerosis and migraine with aura are clinically correlated and both show imaging changes suggestive of myelin disruption. Furthermore, cortical myelin loss in the cuprizone animal model of multiple sclerosis enhances susceptibility to spreading depression, the likely underlying cause of migraine with aura. Since multiple sclerosis pathology involves inflammatory T cell lymphocyte production of interferon-gamma and a resulting increase in oxidative stress, we tested the hypothesis that spreading depression disrupts myelin through similar signaling pathways. Rat hippocampal slice cultures were initially used to explore myelin loss in spreading depression, since they contain T cells, and allow for controlled tissue microenvironment. These experiments were then translated to the *in vivo* condition in neocortex. Spreading depression in slice cultures induced significant loss of myelin integrity and myelin basic protein one day later, with gradual recovery by seven days. Myelin basic protein loss was abrogated by T cell depletion, neutralization of interferon-gamma, and pharmacological inhibition of neutral sphingomyelinase-2. Conversely, one day after exposure to interferon-gamma, significant reductions in spreading depression threshold, increases in oxidative stress, and reduced levels of glutathione, an endogenous neutral sphingomyelinase-2 inhibitor, emerged. Similarly, spreading depression triggered significant T cell accumulation, sphingomyelinase activation, increased

*Correspondence Author Tel: (773)-702-0802; Fax: (773)-702-5175 rkraig@neurology.bsd.uchicago.edu.

Authorship

A.D.P., P.E.K., and R.P.K conceived of the project and designed the experiments with the help of H.M.M. and N.K. A.D.P. and R.P.K. wrote the manuscript. All authors participated in performing experiments and correcting a final version of the manuscript.

Potential Conflicts of Interest

The authors (A.D.P., H.H.M., R.P.K.) report a patent pending entitled, “Treatments for Migraine and Related Disorders” that involves nasal administration of insulin-like growth factor to prevent spreading depression. A.D.P., and R.P.K. also report a patent pending entitled, “Exosomes-Based Therapeutics Against Neurodegenerative Disorders” that involves exosomes containing microRNA that promote myelination and prevent spreading depression. All authors report no other conflicts.

oxidative stress, and reduction of grey and white matter myelin *in vivo*. Myelin disruption is involved in spreading depression, thereby providing pathophysiological links between multiple sclerosis and migraine with aura. Myelin disruption may promote spreading depression by enhancing aberrant excitability. Thus, preservation of myelin integrity may provide novel therapeutic targets for migraine with aura.

Keywords

migraine; multiple sclerosis; spreading depression; myelin; T cells; interferon-gamma; sphingomyelinase-2; hippocampal slice cultures; oxidative stress

Introduction

Migraine is a frequently occurring co-morbid condition with multiple sclerosis (MS). Recent clinical evidence indicates a two to three-fold increase in the frequency of migraine in men and women with MS compared to control patients.[1,2] Similarly, brain imaging studies show an association between migraine and MS. Indeed, in a meta-analysis of magnetic resonance imaging (MRI) studies, Bashir and coworkers evaluated the relationship between migraine and white matter abnormalities, infarct-like lesions, and volumetric changes in grey and white matter regions as detected via MRI.[3] They found that MRI signal changes were most strongly correlated with migraine with aura (MwA). Importantly, white matter abnormalities in particular were associated with MwA but not migraine without aura.[3]

Recent work in animals also supports a link between MwA and MS, and suggests a role for myelin and oligodendrocytes in both conditions. In the cuprizone-demyelination model of MS, Merkler and coworkers[4] show enhanced velocity of spreading depression (SD), the most likely underlying mechanism of migraine aura and related headache pain.[5–9]

Demyelination and impaired remyelination in MS and experimental autoimmune encephalomyelitis (an animal model of MS), involve increased production of interferon-gamma (IFNγ) and oxidative stress (OS) as defined by the excessive generation of oxidants in relation to the availability of antioxidants.[10] Like MS, SD increases IFNγ[11] and OS[12–14] levels in susceptible brain tissue. Although SD is not accompanied by irreversible neuronal injury,[15] it is nevertheless a massive perturbation of brain tissue that, when recurrent, may play a role in the conversion of episodic to high frequency and chronic migraine.[16]

Based on aforementioned considerations, we hypothesized that SD disrupts myelin via IFNγ signaling and increased OS. Quantitative real-time PCR assay for gene expression analysis suggested that SD induces slice culture mRNA changes that are consistent with the presence of T cell lymphocytes, and such findings were confirmed by immunostaining for CD6 and IFNγ positive cells. The presence of T cells in mature hippocampal slice cultures provided an *in vitro* neural preparation that enables the necessary microenvironmental control to test our hypothesis. Using this model, we show that SD disrupted myelin sheaths and caused significant, albeit transient, loss of myelin basic protein (MBP), which resolved over the course of 7 days. Removal of T cells (which prevented secretion of IFNγ) and pharmacological inhibition of nSMase2 abrogated the loss of MBP. Similarly, SD in

neocortex *in vivo* triggered significant T cell accumulation, sphingomyelinase activation, increased OS, and reduction of both grey and white matter myelin. Aspects of these results have appeared in preliminary abstract form.[17,18]

Materials and Methods

Animal Use

Animal procedures were approved by the University of Chicago Animal Care and Use Committee, and were conducted in accordance with the guidelines published in the Guide for Care and Use of Laboratory Animals (2011). Wistar rats were obtained from Charles River.

We model SD (i.e., MwA) in hippocampal slice cultures and translate the findings to the *in vivo* condition using neocortical SD in rats. The rationale of this strategy is based on the fact that SD is a well-conserved neural circuit phenomenon that has been demonstrated in a wide array of grey matter structures and in a wide range of animal species[8,19,20] In each instance, the defining electrical characteristics of SD are analogous. Furthermore, microenvironmental conditions in hippocampal slice cultures can be accurately controlled, the cultures are long-lived, and they retain a functionally intact tri-synaptic loop. Thus, the consequences of synaptically-induced SD (as well as interventions to prevent SD) can be studied for days to weeks after SD induction. Also, these cultures retain a neurovascular unit,[21] neuronal vitality after SD,[22] and quiescent astrocytic[23] and microglial states,[24–28] as well as astrocytic and microglial reactivity to SD[24,26–28] and pro-inflammatory cytokine changes[11] like those seen *in vivo*. Of special importance to our work here, SD in hippocampal slice cultures induces OS like that seen in the neocortex after SD. Furthermore, abrogation of OS by pretreatment with insulin-like growth factor-1[14] or interleukin-11[28] equivalently abrogates SD in hippocampal slice cultures *in vitro* and neocortex *in vivo*.[28,29]

Culture preparation and maintenance

While brain slice cultures are a well-accepted biological preparation used to model neurological disease *in vitro*, their use for SD/migraine research has lagged behind, perhaps due to difficulties in reproducibly evoking SD in slice cultures. Our lab has overcome this impediment and established a long-lived and highly reproducible model of SD in hippocampal slice cultures, in part, by allowing cultures to mature *in vitro*.

Hippocampal brain slice cultures are especially well-suited as an *in vitro* model to study the reaction of neural tissue to brain disease. Although they are deafferented, hippocampal slice cultures show typical regional and cellular form and function, consistent with those observed *in vivo*. Importantly, microenvironmental conditions in slice cultures can be accurately controlled over extended periods of time. For these reasons, we used hippocampal slice cultures for proof-of-principle studies that were then translated to the *in vivo* condition.

We have detailed the specifics of how to grow, maintain, and elicit SD in mature hippocampal brain slice cultures elsewhere.[28] These methods involve enhanced prenatal care [28,30–32] and, once cultures reach maturity, maintenance in a serum-free medium to avoid confounding effects of serum constituents. When evoking SD, serum-free medium

gassed with 5% carbon dioxide/balanced air was used in lieu of the standard Ringer's solution gassed with excessive levels of oxygen, which would promote epileptiform behavior.[22]

Untimed pregnant Wistar female rats (12 total pregnant female rats, ten pups per litter; Charles River Laboratories, Wilmington, MA) were single-housed with Enviro-dri paper bedding (Shepherd Specialty Paper, Hubbard, OR) and Nestlets (#NES3600; Ancare, Bellmore, NY). We prepared 350 μm hippocampal slice cultures from Wistar rat pups (P9-P10) of either sex. Slice cultures were initially maintained in a horse serum-based medium,[33] then transferred to serum-free medium after 18 days *in vitro*, and used for experiments between 21–35 days *in vitro*.[13,14,1718,24,28–32] Slice cultures were tested at 21 days *in vitro* and showed ≥ 95% vitality[28,30,31] as evidenced by the dead cell marker Sytox (#S-34860; Invitrogen, Carlsbad, CA).[22]

Several steps in our use of hippocampal slice cultures are important to reliably evoke SD in this preparation. First, we enrich the environment of pregnant rats. This enhances slice culture vitality from 80–85% to ≥ 95%.[32,34,35] Second, we allow cultures to mature *in vitro* for at least 21 days before use, as opposed to using them at 8–13 days. This prevents triggering spreading depolarizations or seizures,[34,35] which would preclude induction of SD. Third, cultures are initially grown in serum-supplemented medium and then transferred to a serum-free medium after 18 days *in vitro*. Fourth, we have shown that cultures require at least 15 mM glucose.[22] Our habit is to use 42 mM glucose, as originally described for preparation of brain slice cultures.[33] Fifth, we do not expose cultures to oxygen levels above that found in room air (~21%), as this tends to provoke seizures which prevents induction of SD.[22] Sixth, we do not use penicillin/streptomycin since this antibiotic combination, provokes seizure activity,[22] whereas, gentamycin does not. Seventh, physiological recordings (as well as all manipulations) are completed while cultures are exposed to serum-free medium, not Ringer's, since the latter reduces culture vitality if used for extended periods. Eight, our serum-free medium contains glutathione, in addition to cysteine, glycine and glutamate which are essential to maintain cellular glutathione levels. The medium also contains ascorbate and tocopherols and the antioxidant enzymes catalase and superoxide dismutase, as noted in the work of Grinberg and coworkers from our lab (Gemini BioProducts Material Data Safety Sheet; Brewer *et al*., 1993).[13,14]

Experimental manipulations in slice cultures

Spreading depression—SD was induced in a static, interface-recording configuration as previously described.[13,14,17,2428] All recordings were made at the genu of the CA3 interstitial pyramidal neuron area using 2–4 μm tip diameter micropipettes filled with 150 mM sodium chloride. First, the normalcy of slice electrophysiological behavior was confirmed by monitoring the interstitial field potential responses to bipolar dentate gyrus electrical stimulation (100 μs pulses at ≤ 0.2 Hz and 5–20 μA). Slices with CA3 field post-synaptic responses ≥ 3mV were used for experiments.

Second, SD was induced by a uniform injection of current [i.e., 10 pulses, 10 Hz (100 μs/pulse)] at 1,000 uA (i.e., 1,000 nC) as previously described.[13] We have established the typical threshold of current delivery needed to evoke slice culture SD in prior

experiments.[13,28] For example, threshold was determined by progressively doubling the amount of applied current [10 pulses, 10 Hz (100 μs/pulse)] beginning with that needed to trigger a half-maximal field potential response from a single stimulus. Currents for SD threshold were applied no faster than once every three minutes and ranged from 10–10,000 μA (10–10,000 nC). The latter current was the highest we were able to apply and does not necessarily indicate a current that successfully induced SD (i.e., SD threshold). This stimulation strategy was used for experiments reported in Figure 2C.[13,28] As reported previously,[14] we chose a non-injurious and uniform ~10-fold increase in current injection of 1,000 uA (i.e., 1,000 nC) as a stereotypic stimulus to reliably trigger recurrent SD.

For experiments in Figure 1, Table 1 and Figure 3, six SDs were triggered every 7–9 minutes over an hour to elicit robust SD-related responses. As previously noted,[14] we use a repetitive epoch of SDs to model high frequency and chronic migraine in order to replicate the hyperexcitable phenotype seen in the brain of migraineurs.[36–40]

Control slice cultures were placed in electrophysiological recording unit for one hour, with evoked standard field potentials instead of SD.

T cell lymphocyte depletion—T cells in slice cultures were depleted via incubation with a neutralizing dose (10 μg/mL) of anti-CD4 (mouse anti-rat; clone OX-38; isotype IgG2a) antibody (#MCA372G; AbD Serotec, Oxford, UK) at nine days *in vitro* for three days. Control cultures were treated with mouse IgG2a isotype control (#MG2a00; Invitrogen). T cell ablation was confirmed by immunostaining slices for presence of CD6-positive cells (see below) versus isotype control-treated cultures. Slice viability was assessed prior to use at 21 days *in vitro*, using the dead-cell fluorescent marker Sytox as previously described.[22] Anti-CD4 treatment did not elicit any evidence of neural cell death (data not shown).

Interferon gamma treatment—Recombinant rat IFNγ (#585-IF; R&D Systems, Minneapolis, MN) was used at a physiological dose of 500 U/mL (0.5 μL/mL). 500 U/mL did not result in any evidence of cell injury in slice cultures as measured via Sytox, yet was a sufficient stimulus to initiate an adaptive response.[41] Slices were exposed to IFNγ for the indicated amounts of time, then fixed for immunostaining or harvested for protein extraction.

Neutral sphingomyelinase-2 inhibition—GW4869 (#567715; Calbiochem, La Jolla, CA), a specific nSMase2 inhibitor, was used at 10 μM in recording medium.[42] For determination of MBP changes after SD, slices were pre-incubated with GW4869 for one hour, followed by induction of six SDs in normal medium. The slices were then returned to GW4869-containing serum-free medium for 24 hours before being harvested for protein extraction. For evaluation of MBP levels after stimulation with IFNγ, cultures were pre-incubated with GW4869 for one hour then transferred to serum-free medium containing both GW4869 and IFNγ (500 U/mL) for 24 hours. Slices were then washed and transferred to GW4869-containing serum-free medium for one day before harvest for protein extraction.

Electron microscopy

Fixative for electron microscopy (EM) as previously described[30,31] consisted of the following: 4% paraformaldehyde, 2.5% glutaraldehyde, and 0.1 M sodium cacodylate buffer (pH 7.4). Slice cultures were fixed at room temperature for 10 minutes followed by overnight fixation at 4°C before embedding and sectioning. Whole animals were anesthetized with ketamine/xylazine (80 mg/kg and 7.5mg/kg respectively, delivered by intraperitoneal injection) and euthanized by intracardiac perfusion with room temperature solutions of 0.1 mL 0.05% EDTA/saline, followed by 250mL of saline and finally 250 mL of EM fixative. Brains were removed and post-fixed at room temperature for 10 minutes followed by overnight fixation at 4°C before embedding and sectioning. EM for visualization of myelin sheath integrity was performed from slice cultures sectioned perpendicular to Schaffer collateral and CA1 output axons at CA3, and rat brains were sectioned at a 45 degree angle to the vertical of the transverse axis at the paramedian neocortex (~ 4 mm caudal to Bregma). Images were acquired using the University of Chicago Electron Microscopy Core Facility, and the extent of myelin disruption was quantified (i.e., the number of cells with myelin disrupted per total cells counted).

Gene expression studies

Tissue collection—Samples were collected and processed as previously described.[43,44] Briefly, slice culture inserts were submerged in 3 mL RNA*later* (#AM7021; Ambion, Carlsbad, CA). The CA3 hippocampal region was dissected out of slices with a glass knife (#10100-00; Fine Science Tools, Foster City, CA), and harvested in 1 mL of cold sterile PBS in RNase/DNase free 1.5 mL microcentrifuge tubes. PBS supernatant was then removed and slices resuspended in 500 μL of cold TRIzol reagent (#15596026; Ambion). Samples were incubated for five minutes at room temperature, then used immediately or stored at −80°C. Total RNA isolation was performed using a combination of TRIzol and Qiagen's RNeasy Micro Kit columns (#74004; Qiagen, Valencia, CA). Quantification of RNA was performed using RiboGreen (#R-11491; Invitrogen) according to the manufacturer's protocol.

qPCR—Inflammatory cytokine expression after SD versus control was assayed via PCR arrays directed against a focused panel of genes involved in inflammation (RT^2 Profiler™ PCR Array #PARN-011A, PARN-021A; SABiosciences, Frederick, MD) run on a real-time iCycler™ PCR platform (Bio-Rad, Richmond, CA). Briefly, cDNA was synthesized using RT^2 first strand kit (#C-03; SABiosciences), and real-time PCR was performed using SuperArray RT^2 SYBR Green qPCR Master Mix (#330510; SABiosciences). Thermocycling protocol was as follows: 95°C for 10 minutes, followed by 40 cycles of amplification at 95°C for 15 seconds, 60°C for 60 seconds. Melting curves were run for all plates. Relative gene expression normalized to ribosomal protein L13a (Rpl13a) was calculated using the RT^2 Profiler PCR Array Data Analysis version 3.4 software (SABiosciences). Fold changes of greater than two were taken to be significant.[43–45] For assaying IFNγ in slice cultures, which contain ~50 T cells each, cDNA was pre-amplified using the RT^2 PreAMP cDNA (#PBR-011A; SABiosciences) and a real-time rat IFNγ primer assay (#PPR45050C; SABiosciences).

Immunohistochemical and histochemical staining

Slice cultures were fixed and processed for immunohistochemical staining as previously described[43] with few modifications. Briefly, slices were fixed overnight in periodate-lysine-paraformaldehyde fixative.[46] The next day, slices were rinsed in PBS and then incubated in 95% acetic acid/5% ethanol for 20 minutes. Negative controls in all experiments excluded incubation with the primary antibody. After blocking in 10% goat serum (#16201-064; Gibco, Grand Island, NY), slice cultures were incubated with primary antibody overnight at 4°C. After 3 rinses in PBS, slices were incubated in secondary antibody for one hour at room temperature and staining was visualized with 3,3'-diaminobenzidine (#D8001-1G; Sigma-Aldrich, St Louis, MO), cleared and coverslipped using Permount (#SP15100; Fisher Scientific, Fair Lawn, NJ). Sections were stained using anti-MBP (#18-0038; Zymed), or anti-IFNγ (#ARC4033; Invitrogen), followed by the appropriate HRP conjugated secondary antibody [anti-rabbit (#G21234; Invitrogen) and anti-mouse (#G21040; Invitrogen), respectively]. For IFNγ staining, slice cultures were pre-treated with lipopolysaccharide (10 μg/mL x 24 hours; #L4774; Sigma) to stimulate T cells.

MBP immunostaining was quantified using digital imaging strategies to assess integrated optical density.[46] The area of interest was restricted to the CA3 pyramidal neuron layer as illustrated in Figure 2, but using bright field illumination with details described below for glutathione quantification.

T cell fluorescent immunohistochemical staining followed the same procedures as above, staining with anti-CD6 (#MCA339R; AbD Serotec; a pan T cell marker) followed by fluorescent secondary antibody (#A-11001, Goat anti-mouse IgG; Invitrogen). Slides were coverslipped using ProLong Gold Antifade reagent (#P36930; Invitrogen).

Microglia were labeled after fixation with 10% phosphate buffered formalin (#SF100-4; Fisher Scientific) using the fluorophore-tagged isolectin-GS-IB_4 (#I21411 from Griffonia simplicifolia, Alexa Fluor® 488 conjugate; Invitrogen).[24]

Western blots

Expression of MBP in hippocampal slice culture samples was evaluated using standard SDS-PAGE and immunoblotting procedures. Briefly, equal amounts of total protein (20 μg) hippocampal slice culture homogenates were loaded to SDS-PAGE gels for separation, transferred to nitrocellulose membrane, and immunolabeled for MBP (#NBP1-05203; Novus Biologicals, Littleton, CO) with β-actin (#A5316; Sigma-Aldrich) as a loading control. β-actin was chosen as a loading control, as its protein levels do not change with spreading depression (unpublished observation). Blots were visualized by standard chemiluminescence and densitometric quantification performed with Quantity One 1-D Analysis Software (#170–9600; Bio-Rad). MBP was quantified using all three bands: 21.5, 18.5, and 17.2 kDa.

Oxidative stress quantification

CellROX Deep Red Reagent (#C10422; Invitrogen), a cell-permeant fluorogenic probe, was used as previously described to assess OS.[13,14] Slices were exposed to IFNγ (500 U/mL ×

12 hours) as an initial OS-producing stimulus, then incubated for one hour with CellROX (acute OS response). CellROX fluorescence intensity was quantified via digital imaging strategies as described below. A standardized area of interest at the CA3 pyramidal neuron layer was used for all quantifications.

Protein carbonyl quantification

A Protein Carbonyl Content Assay Kit (#ab126287; Abcam, Cambridge, MA) was used according to manufacturer's protocol for measurement of protein carbonylation as a readout of OS in rat brains after whole animal SD. Briefly, protein was extracted from the neocortex of animals exposed to KCl-induced SD or controls using RIPA buffer as previously described.[30] Protein homogenate was treated with Streptozocin to remove any nucleic acid contaminates and reacted with 2, 4-Dinitrophenylhydrazine, followed by quantification of the acid hydrazones at 405 nm. BCA assays (#23225; ThermoFisher Scientific, San Jose, CA) were simultaneously run and a standard curve constructed for the calculation of protein carbonyl content based on optical density.

Glutathione quantification

ThiolTracker (#T10095; Invitrogen) is a fluorescent dye that reacts with reduced thiols in intact cells and thus is an excellent marker for glutathione, which is the most prevalent cellular thiol.[47] Procedures for staining followed those of the manufacturer, modified for use with hippocampal slice cultures. ThiolTracker was dissolved in dimethyl sulfoxide (2 mM) and used at 20 μM in a thiol-free solution. Briefly, cultures inserts were dipped into three separate 60 mm culture dishes containing 10 mL/each of Gey's balanced salt solution [(#G9779; Sigma) supplemented with 7.25 mL 45% glucose (#G8769; Sigma)] to remove extracellular thiols. Inserts containing cultures were then incubated in Gey's supplemented with glucose and containing ThiolTracker pre-equilibrated to normal incubation conditions which was continued for 30 minutes. Inserts were then washed again as described above and fixed in 10% phosphate buffered formalin at 4°C overnight, mounted, and coverslipped as described above for fluorescence immunostaining procedures.

Glutathione was quantified using a self-calibrating sensitive CCD digital imaging system consisting of a QuantEM-512SC camera (Photometrics, Tucson, AZ), electronic shutter (Lambda SC Smart Shutter; Sutter Instruments, Novato, CA), standard 100 watt Hg light on a DMIRE2 inverted microscope (Leica Microsystems Inc., Buffalo Grove, IL) at 20x gain. A standardized area of interest at the CA3 pyramidal neuron layer was used for all quantifications. Resultant digital images were thresholded to a range applied to all images and the average optical intensity registered using MetaMorph software (ver. 7.5.4.0; Molecular Devices, Sunnyvale, CA).

Representative confocal images of control microglia-ThiolTracker staining were acquired using a Leica TCS SP5 II AOBS laser scanning confocal microscope (University of Chicago Integrated Microscopy Core Facility). Imaging section thickness was 772 nm to reduce potential cell body overlap. Images were acquired at 63x gain (1024 × 1024 pixels @ 12-bit). Alexa Fluor® 594 tagged isolectin excitation/emission parameters were 561/576–655 nm and while those for ThiolTracker were 488 nm/510–533 nm.

Whole animal electrophysiology

Whole animal SD recordings were completed using aseptic techniques, as previously described[46,48,49] and recently updated.[28] Briefly, male Wistar (300–400 gm) rats were anesthetized with isoflurane in oxygen (5% induction, 3% during surgical procedures, and 2–3% during recordings) via an inhalational mask and mounted in a standard table-top nose clamp with ear bars and kept warm with an overhead infrared lamp to keep core temperature at 37°C. Eyes were coated with Artificial Tears (#17478-062-35; Akorn, Lake Forest, IL) and the head shaved and cleansed with Betadine (Purdue Pharma, Stamford, CT). Next, 0.05 mL Bupivacaine (#0409–4272-01; Hospira, Lake Forest, IL) was injected subcutaneously to both sides of the surgical site, and a midline scalp incision was made from just behind the eyes to the lambdoid suture area. Two 1–2 mm craniotomies were made: a stimulation craniotomy at −2.0 mm from Bregma and 1.5 mm to the left of the sagittal suture, and a recording craniotomy at −6.0 mm from Bregma and 4.5 mm lateral to the sagittal suture. Craniotomies were performed under saline cooling and without damaging the underlying dura.

Anesthetized animals were then transferred to a stereotaxic recording setup where gaseous anesthesia (1.5–2.0% isoflurane remainder oxygen), oxygen monitoring, and warming were continued. The skull was warmed (37°C) directly with sterile saline superfusion. For interstitial DC recordings, a 2–4 μm tip microelectrode was placed 750 μm below the pial surface with a Canberra micromanipulator (Narishige, Long Island, NY) and recordings begun using an Axoprobe A1 amplifier system and Digidata 1440A analog-digital conversion board. For KCl-induced SD threshold measurements, a microelectrode with tip broken to 8–12 μm (1.0 mm outside diameter, 0.58 mm inside diameter; Sutter Instrument, Novato, CA) and filled with 0.5M KCl was positioned 750 μm below the pial surface. Micro-injections of KCl were administered via pressure from a Picospritzer-II electronic valve system (Parker, Hollis, NH), whose injection periods were registered directly to the permanent digital recording of SD induction.

In prior experiments, injection electrodes were raised immediately after SD induction and moved into a microscope slide with depression wells (ThermoFisher Scientific) filled with light 3-In-ONE oil (WD-40 Company, San Diego, CA). KCl injections were then repeated into oil and volumes calculated from diameter measured using a compound microscope fitted with an optical micrometer within an eye piece.[28,29] Here, we increased this nL volume by 2–3 fold to reliably evoke six SDs. Right neocortex, which did not experience SD, was used for control measurements.

Neutral Sphingomyelinase Assay

nSMase2 activity in rat brain was determined using a Neutral Sphingomyelinase Assay Kit (#K-1800; Echelon, Salt Lake City, UT) according to the manufacturer's protocol. Briefly, brain tissue was homogenized in cold lysis buffer (1% Triton X-100, 150 mM NaCl and 25 mM Tris-HCl, pH 7.4). Samples were diluted to 250ng/μL and 100μL (25 μg) was incubated with Reaction Mixture (5x Enzyme Mix, DAOS, Sphingomyelin, Choline Oxidase, Sphingomyelin Reaction Buffer [0.05 M Tris-HCl, 10 mM $MgCl_2$, 0.66 mM $CaCl_2$, pH

7.4]) at 37°C with agitation for four hours, then read at 595 nm. Data was analyzed using GraphPad Prism (v.6.0; GraphPad Software, Inc. San Diego, CA).

Statistical methods

Data were analyzed using SigmaPlot software (v. 12.5; Systat Software, San Jose, CA). All data were subject to normality testing (*p*-value to reject: 0.05), equal variance testing (*p*-value to reject: 0.05), and power (1-β: > 0.8). Controls in each experiment were set to 1.0 with experimental data scaled proportionally to better allow inter-experiment comparisons. Molecular biological data (mRNA and Western blot protein) analyses included two technical replicates per experimental measurement. All experimental groups consisted of biological replicates of $n \geq 3$. All experimental samples were compared to age-matched controls (or contralateral neocortical controls). Statistical tests are noted in the figure legends.

Results

Myelin disruption from spreading depression *in vitro*

The effect of SD on astroglia and microglia are well-recognized. SD evokes a transient astrogliosis that lasts weeks,[11,48] and also activates microglia.[13,14,24,26,27,46,50] SD can shift the cell fate of progenitor NG2 cells from oligodendrogenesis to astrogenesis,[51] but little is known about the effect of SD on oligodendrocytes. As a first approach to the latter, we focused on IFNγ and OS effects on myelin.

SD was elicited in slice cultures (Fig. 1A). Western blots (Fig. 1B) show that SD elicited a significant initial loss of MBP that progressively recovered to control levels by seven days after SD. Specific values were: Control: 1.00 ± 0.05 (n = 14); one day: 0.54 ± 0.05 (n = 5); three day: 0.76 ± 0.07 (n = 4); and seven day: 1.00 ± 0.04 (n = 18).

The loss of MBP was reflected in a significant disruption of the myelin sheath, as evidenced via electron microscope images. Little indication of myelin sheath disruption was seen in control culture images (Fig. 1C). In contrast, one day after SD, there were frequent disruptions consisting of splitting of myelin lamellae at intraperiod lines between major dense lines, consistent with that seen in experimental autoimmune encephalomyelitis [52,53] (Fig. 1D). However, seven days after SD the disrupted myelin sheaths had recovered. The extent of myelin damage was quantified from EM images by counting the number of axons with myelin disruptions per total cells counted (Fig. 1E) [Specific values: Control: 1.00 ± 0.22; one day after SD: 2.53 ± 0.02; seven days after SD: 1.14 ± 0.11 (ten images per slice, n = 3 slices /group)]. Similarly, densitometric assessment of immunostaining intensity for MBP in the CA3 area of slice cultures (ten images per slice, n = 3 slices /group) showed SD triggered a significant loss of MBP after one day [with specific values of 1.00 ± 0.20 and 0.11 ± 0.02] (Fig. 1F–H). Similar reductions in MBP immunostaining after SD were seen, though not quantified, in other hippocampal slice regions.

T cell/IFNγ-mediated effects of spreading depression involve sphingomyelinase

Considering the extensive evidence for involvement of T cells/IFNγ in central nervous system demyelination, including gray matter demyelination,[54] we probed slice cultures for

the presence of T cells, which can survive for months.[55] A quantitative real-time PCR assay for inflammatory cytokine gene expression revealed that several mRNA species indicative of the presence of T cells[45] increased 2.5–11.0 fold three hours after six SDs (Table 1).

Next, we verified the presence of T cells and their production of IFNγ in hippocampal slice cultures. Immunostaining for CD6 (a pan T cell marker not expressed on CNS cells), revealed an average of 52 ± 6 T cells (n = 9; Fig. 2A) per slice culture. This is a seemingly small number compared to the ~100,000 cells that constitute each slice (estimated from total RNA/slice assuming 5–20 pg/mammalian brain cell[24,56]), but they are able to produce biologically relevant products. These cells could be functionally activated by lipopolysaccharide to secrete IFNγ (Fig. 2B) and thus influence slice culture activity. Relative cell counts (from ten images per slice) were: Control: 1.00 ± 0.12 (n = 3) and after lipopolysaccharide stimulation: 1.98 ± 0.13 (n = 7).

SD reduces the threshold to subsequent SD,[13,14] an effect that involves increased expression of tumor necrosis factor-alpha (TNFα) and OS.[14] Application of IFNγ to naïve slice cultures for 24 hours mimicked effects seen following SD, increasing brain slice excitability and OS.[57] One day after continuous exposure to IFNγ, SD threshold was significantly reduced (n = 5/group) from 1.00 ± 0.09 to 0.05 ± 0.01 (Fig. 2C). Similarly (n = 5/group), after three to seven hours of continuous exposure to IFNγ, slice culture OS was significantly increased from 1.00 ± 0.07 to 1.50 ± 0.27 (Fig. 2D–G). This increased OS was reflected in reduced slice culture levels of the antioxidant glutathione, as measured via ThiolTracker (Fig. 2H–K). Specifically: Control: 1.00 ± 0.08 (n = 12) and IFNγ-exposed: 0.66 ± 0.07 (n = 9). Changes in glutathione levels were most evident in microglia (Fig. 2J).

Since IFNγ stimulates the release of TNFα from microglia,[58] and TNFα treatment significantly decreases MBP levels in slice cultures [Control: 1.00 ± 0.05; TNFα: 0.65 ± 0.07 (n =6/group)], next determined whether IFNγ itself influenced slice culture MBP levels. Exposure to 500 U/mL IFNγ for one day triggered a significant decline in MBP that was amplified by inclusion of TNFα [Control: 1.00 ± 0.17; IFNγ: 0.70 ± 0.10; IFNγ + TNFα: 0.32 ± 0.05 (n = 6/group)] (Fig. 3A). Furthermore, continuous exposure to IFNγ led to a significant ($p \leq 0.001$) and progressively severe decline in MBP (n = 6/group: three days: 0.45 ± 0.04; seven days: 0.18 ± 0.05; data not shown).

We next incubated slice cultures with anti-CD4 antibody to deplete T cells.[59] Immunostaining for CD6 confirmed that the neutralizing antibody significantly ($p < 0.001$) ablated T cells [Control: 1.00 ± 0.10 (n = 11); anti-CD4: 0.08 ± 0.02 (n = 5)]. Mouse IgG2a (isotype control) had no impact on T cell counts. Anti-CD4 treatment also dramatically reduced IFNγ mRNA three hours after 6 SDs. While SD in untreated cultures (n = 6/group) triggered a 4.65-fold rise in IFNγ compared to controls, SD in anti-CD4 treated slices (n = 3/group) resulted in a two-fold reduction in IFNγ compared to controls (anti-CD4 treatment without SD), indicating a baseline presence of IFNγ-secreting T cells. Application of anti-CD4 antibody for removal of T cells had no impact on MBP when there was no exposure to SD, and prevented the drop in MBP normally seen one day after SD [Control: 1.00 ± 0.18 (n = 3); anti-CD4: 0.79 ± 0.16 (n = 3); anti-CD4+SD: 0.87 ± 0.08 (n = 3)] (Fig. 3B). Finally, since TNFα activates nSMase2[42,60] which promotes demyelination, we examined how

pharmacological inhibition of nSMase2 activity (via GW4869)[61] impacted MBP loss from SD. Pretreatment with GW4869 prevented the drop in MBP seen after SD or with 24 hour IFNγ treatment [Control: 1.00 ± 0.11 (*n* = 9); GW4869: 1.34 ± 0.16 (*n* = 8); GW4869+SD: 1.30 ± 0.11 (*n* = 3); GW4869+IFNγ: 0.79 ± 0.15 (*n* = 5)] (Fig. 3C), indicating that TNFα acts through nSMase2 to damage myelin. GW4869 alone had no impact on MBP levels.

Myelin disruption from spreading depression *in vivo*

The above *in vitro* results could be recapitulated *in vivo*. Exposure to six recurrent neocortical SDs (Fig. 4A) resulted in significant structural disruption of myelin one day later, as demonstrated by EM [Control: 1.00 ± 0.12 ; SD: 3.35 ± 0.34 (ten images per animal, *n* = 3 animals /group)] (Fig. 4B–D). There was also a significant increase in neocortical nSMase activity one day later [right, control neocortex: 1.00 ± 0.22; left, SD-exposed neocortex: 1.60 ± 0.09 (*n* = 4 animals/group)] (Fig. 4E). Similarly, six neocortical SDs significantly reduced MBP immunostaining in grey matter (Fig. 4F–H), and importantly, in underlying white matter of the lateral corpus callosum (Fig. 4I–K), as a representative zone of white matter myelin. Specific values, measured via densitometry were: Control: 1.00 ± 0.06 versus SD: 0.36 ± 0.06 in neocortical grey matter, and Control: 1.00 ± 0.01 versus SD: 0.53 ± 0.07 in corpus callosum (ten images per animal, *n* = 4 animals /group). Finally, we found that similar to seizures,[62] SD increased CNS recruitment of lymphocytes. Immunostaining for CD6 (Fig. 4L–N) revealed significantly increased T cell counts in SD-exposed neocortex [Control: 1.00 ± 0.03, SD: 2.29 ± 0.25 (ten images per animal, *n* = 3 animals /group)]. Furthermore, exposure to SD significantly increased production of IFNγ (Fig. 4 O–Q) by these cells [Control: 1.00 ± 0.19, SD: 6.90 ± 0.06 (ten images per animal, *n* = 3 animals /group)], suggesting that SD increases CNS infiltration of activated T cells *in vivo*.

Discussion

The present findings reveal that both *in vitro* and *in vivo*, SD triggered transient disruption of myelin that resolved a week later. This damage involved production of IFNγ by T cells and was accompanied by increased OS, glutathione depletion, and activation of nSMase2. MS also shows evidence of these changes, which begins to provide a pathophysiological link for clinical evidence correlating disruption of myelin in patients suffering from MwA and MS.[1–3]

The literature provides precedent for our observations, reporting a similar transient disruption of myelin in response to a variety of insults. One study shows similar ultrastructural damage to myelin sheaths and loss of MBP following hippocampal seizure.[63] Another reports loss of MBP in hippocampus 90 minutes post-exposure to carbon monoxide, which recovered within 14 days.[64] Interestingly, they also show MBP colocalized with ED1+ cells (microglia / macrophages) at one day post-injury, suggesting rapid clearance by resident myeloid cells. Conversely, Liu and co-workers show rapid (within hours) calpain-mediated proteolysis of MBP by oligodendrocytes in a model of traumatic brain injury,[65] suggesting multiple routes of MBP degradation.

The current understanding is that newly proliferated oligodendrocytes are necessary for remyelination. While that might also be the case in SD, much of the research on remyelination has been done in models where more extensive myelin damage and oligodendrocyte death is evident.[66,67] Little is known about the capacity for myelinating oligodendrocytes to recover from subtle damage, as seen from SD. However, in a model of ischemic injury, McIver *et al*., show evidence of endogenous repair that occurs rapidly (between 48 hours and one week) and that is not completely mediated by proliferating cells. In this study, they show that despite extensive oligodendrocyte death, adult oligodendrocytes can survive ischemic injury and may recover intact processes, thus contributing to repair mechanisms in conjunction with post-mitotic oligodendrocyte precursor cells already present around injury sites.[68] Additional studies will be necessary to determine the source of myelin repair in SD, and whether minor structural damage can be repaired by a previously injured but still viable oligodendrocyte.

To our knowledge, this is the first study to examine the role of myelin (and by extension, oligodendrocytes) in SD. We provide direct evidence that SD disrupts myelin. Prior studies have indirectly pointed to potential involvement of axons, and may have been observing the result of damage to surrounding myelin. It has long been recognized that susceptible brain grey matter is necessary for initiation and propagation of SD, with SD *per se* rarely crossing beyond white matter boundaries.[19] Trans-synaptic SD initiation is preceded by a volley of neuronal hyperexcitability that is sufficiently robust to synchronously involve an adequate tissue volume.[69–71] This hyperexcitability causes current flow into principal neurons, resulting in depolarization that slowly propagates.[69,70] As this principal neuron depolarization recovers (and cellular impedance returns toward normal), the interstitial DC potential swings positive where SD occurred [as current flows out (e.g., see Fig 4A, late DC records)], and is often evident in the contralateral neocortex as a small negative deflection.[46] These SD-recovery interstitial field potentials may be due to layer III and/or layer IV principal neuron core conductor behavior, since these cells send their axon terminals to contralateral neocortex.

Other examples indicate that brain regions remote from the zone undergoing SD are also affected. Recurrent neocortical SD causes local astrogliosis, which is also evident remotely in ipsilateral basal ganglia where SD did not occur.[48] Cyclooxygenase-2 immunostaining increases within SD-affected neocortex, but also increases in ipsilateral hippocampal regions.[46] Furthermore, SD triggers remote functional changes. Neocortical SD causes changes in local blood flow that are also seen in ipsilateral hippocampus. Similarly, SD in hippocampus changes blood flow in overlying neocortex.[49] SD itself can be made to propagate from entorrhinal cortex to hippocampus in acute brain slices.[71] Finally, neocortical SD can be made to spread into subcortical structures, including hippocampus and thalamus,[72] or into striatum,[73,74] *in vivo*.

These examples show that SD triggers remote effects in regions interconnected by myelinated axons, but do not directly implicate involvement of myelin. Prior evidence for myelin disruption in migraine (and by extension SD) is exemplified by MRI of patients with ophthalmoplegic migraine, showing transient demyelination of the oculomotor nerve.[75–79] Thus, myelin *is* disrupted by migraine and, as we show here, by SD.

We next asked how myelin disruption impacts SD. As with seizures, frequent migraine increases the likelihood of subsequent attacks that may develop into high frequency, chronic migraine.[80–83] Our experiments showed that increased susceptibility to SD was correlated with increased myelin disruption, which could enhance brain excitability. Excessive brain excitability is the underlying cause of SD/migraine susceptibility. The brains of migraineurs are hyperexcitable.[84] Migraineurs have reduced cortical inhibition[36] and increased excitability between headaches.[36–38,85] Interictal hyperexcitability could lower SD threshold in MwA patients [86,86–88] and in animals used to model migraine with SD.[20,89–92] Occipital cortex hyperexcitability[39,9294] and slowly propagating changes, as seen in SD, are also seen in patients suffering from migraine without aura. [95–97] Thus, hyperexcitability may also be an aspect of migraine without aura.

Channelopathies have often been cited as a cause of aberrant hyperexcitability that initiates SD.[88,89,92] While this work is informative, results may be applicable to only a subset of migraineurs, such as those suffering from hemiplegic migraine. Furthermore, it is not clear how SD/migraine threshold can be reduced by recurrent attacks of SD/migraine via channelopathies. Our prior work has shown that SD begets SD via increased microglial secretion of TNFα and related increases in OS.[13,14] The SD-induced changes in microglia can be abrogated via application of insulin-like growth factor-1, which as a result increases SD threshold.[13,14] Results presented here suggest a novel process by which increased frequency of SD/migraine may promote subsequent attacks. Demyelination that occurs in the cuprizone model of MS increases susceptibility to SD[4] as well as hippocampal seizures.[98] We suggest that myelin disruption within grey matter may promote SD susceptibility by increasing local hyperexcitability via ephaptic transmission (*i.e*., electrical crosstalk).

In light of the clinical correlation between MS and MwA,[1–3] we explored how T cells, their release of IFNγ, and related OS could impact myelin in SD. T cells, which are important to the pathogenesis of MS, significantly increased in number following exposure to recurrent SD. Conversely, removing T cells from slice culture abrogated the disruption of myelin that occurs with SD. Although the mechanisms of T cell trafficking into brain following SD are unknown, T cell counts are elevated in the blood of patients with migraine[99] and seizure.[62] Seizures also occur with an initial excessive hyperexcitability and are known to increase T cell entry to brain.[99] T cells also generate IFNγ, and levels of this cytokines rise both in slice cultures[11] and in whole animal brains after exposure to SD. Exposure of microglia to the Th1 cytokine IFNγ induces their production of TNFα, as part of the well-recognized pleiotropic and redundant innate cytokine cascade first recognized in the periphery.[100] IFNγ and TNFα cooperatively promote generation of OS in neural tissue,[101] consistent with our finding that additive treatment with both cytokines reduced MBP to a greater degree than either alone. Treatment with either IFNγ or TNFα alone reduced slice culture MBP by ~30%. Treatment with both cytokines increased this loss of myelin to ~68%, as would be the expected behavior of an interactive cascade. Furthermore, IFNγ significantly accelerates proteolysis of MBP,[102] suggesting a mechanism for the rapid loss of MBP following SD. Notably, migraine, like SD, occurs with increased OS.[103]

Reactive oxygen species and pro-inflammatory cytokines converge upon activation of nSMase2-ceramide pathways. IFNγ stimulates the release of pro-inflammatory factors including TNFα, which depletes intracellular glutathione[104] and activates nSMase2. Conditions of high OS likewise deplete glutathione,[105] but reactive oxygen species can also directly activate kinases that induce nSMase2.[106,107] We show that SD increases nSMase2 activity and induces myelin disruption. Pharmacological inhibition of nSMase2 prevents myelin damage, suggesting a pathway for transient myelin damage in the context of SD.

Myelin contains neutral sphingomyelinases[60] whose activity may be enhanced by SD, leading to sphingomyelin hydrolysis, ceramide formation and other downstream reactions with deleterious effects on myelin integrity. The lipid composition of normal myelin consists of a high proportion of long-chain sphingolipids to polyunsaturated lipids, and dysregulation can lead to decompaction of myelin sheaths.[108] In fact, sphingomyelin content is three-fold lower than normal in myelin bilayers from a model of MS, and there is a direct correlation between the lipid content and MBP adsorption mechanisms that affect adhesion of opposing myelin leaflets.[109] This is consistent with our results showing a rapid loss of MBP that recovers in only a few days, and EM that exhibits relatively intact myelin sheaths with localized areas of decompaction. Often used as a readout of myelination, MBP is a major protein component of myelin. It is required for compaction of oligodendrocyte membrane processes into a tight sheath and subsequent maintenance of this multilamellar structure.[110] MBP-deficient shiverer mice are severely hypomyelinated, and possess morphologically abnormal myelin sheaths,[111] demonstrating the importance of MBP. Conversely, exposure to environmental enrichment (i.e., volitionally increased intellectual, social and physical activity) protects against SD[28] and involves increased myelination,[112] lending further support to our hypothesis.

Conclusions

In summary, we have shown that SD-induced increased release of pro-inflammatory cytokines (IFNγ/TNFα) resulted in OS that activated nSMase2, leading to transient disruption of myelin sheaths. SD-induced disruption of myelin may increase SD susceptibility by enhancing excitability through aberrant cross-talk between newly demyelinated nerve fibers. Taken together, these results indicate a role for oligodendrocytes and myelin in the pathogenesis of SD and MwA.

Acknowledgement

This work was supported by the National Institutes of Health Common Fund, through the Office of Strategic Coordination/Office of the Director (1-UH2 TR000918), core facilities funds from the National Center for Advancing Translational Sciences of the National Institutes of Health (UL1 TR000430), the National Institute of Neurological Disorders and Stroke (NS-019108), the National Institute of Child Health and Human Disorders (5 PO1 HD 09402), National Institutes of General Medicine training grant (5T32GM007839-31) (A.D.P.), an Illinois Pilot grant from the National Multiple Sclerosis Society (IL-0009). N. Klauer was partially funded by the Dimensions Center for the Science and Culture of Healthcare from Cornell College.

We thank Drs. D. Gozal, B. Popko, A, Reder, K.M. Pusic, and L. Won for reading and commenting on the manuscript. We also thank Drs. L. Won and Y. Chen for assistance with immunostaining and electron microscopy, respectively. Electron microscopy was performed at the University of Chicago Electron Microscopy Facility

ABBREVIATIONS

EM	electron microscopy
IFNγ	interferon-gamma
MRI	magnetic resonance imaging
MwA	migraine with aura
MBP	myelin basic protein
MS	multiple sclerosis
OS	oxidative stress
SD	spreading depression
TNFα	tumor necrosis factor alpha

References

1. Kister I, Caminero AB, Monteith TS, et al. Migraine is comorbid with multiple sclerosis and associated with a more symptomatic MS course. J Headache Pain. 2010; 11:417–425. [PubMed: 20625916]
2. Pakpoor J, Handel AE, Giovannoni G, Dobson R, Ramagopalan SV. Meta-analysis of the relationship between multiple sclerosis and migraine. PLoS One. 2012; 7:e45295. [PubMed: 23024814]
3. Bashir A, Lipton RB, Ashina S, Ashina M. Migraine and structural changes in the brain: a systematic review and meta-analysis. Neurology. 2013; 81:1260–1268. [PubMed: 23986301]
4. Merkler D, Klinker F, Jurgens T, et al. Propagation of spreading depression inversely correlates with cortical myelin content. Ann Neurol. 2009; 66:355–365. [PubMed: 19798729]
5. Leao AAP. Spreading depression of activity in the cerebral cortex. Journal of Neurophysiology. 1944; 7:359–390.
6. Milner PM. Note on a possible correspondence between the scotomas of migraine and spreading depression of Leao. Electroencephalogr Clin Neurophysiol. 1958; 10:705. [PubMed: 13597818]
7. Moskowitz MA, Nozaki K, Kraig RP. Neocortical spreading depression provokes the expression of c-fos protein-like immunoreactivity within trigeminal nucleus caudalis via trigeminovascular mechanisms. J Neurosci. 1993; 13:1167–1177. [PubMed: 8382735]
8. Pietrobon D, Moskowitz MA. Pathophysiology of migraine. Annu Rev Physiol. 2013; 75:365–391. [PubMed: 23190076]
9. Noseda R, Burstein R. Migraine pathophysiology: anatomy of the trigeminovascular pathway and associated neurological symptoms, cortical spreading depression, sensitization, and modulation of pain. Pain. 2013; 154(Suppl 1):S44–S53. [PubMed: 23891892]
10. Espejo C, Penkowa M, Saez-Torres I, et al. Interferon-gamma regulates oxidative stress during experimental autoimmune encephalomyelitis. Exp Neurol. 2002; 177:21–31. [PubMed: 12429207]
11. Kunkler PE, Hulse RE, Kraig RP. Multiplexed cytokine protein expression profiles from spreading depression in hippocampal organotypic cultures. J Cereb Blood Flow Metab. 2004; 24:829–839. [PubMed: 15362713]
12. Viggiano A, Viggiano E, Valentino I, Monda M, Viggiano A, De Luca B. Cortical spreading depression affects reactive oxygen species production. Brain Res. 2011; 1368:11–18. [PubMed: 20974112]
13. Grinberg YY, van Drongelen W, Kraig RP. Insulin-like growth factor-1 lowers spreading depression susceptibility and reduces oxidative stress. J Neurochem. 2012; 122:221–229. [PubMed: 22524542]

14. Grinberg YY, Dibbern ME, Levasseur VA, Kraig RP. Insulin-like growth factor-1 abrogates microglial oxidative stress and TNF-alpha responses to spreading depression. J Neurochem. 2013; 126:662–672. [PubMed: 23586526]
15. Nedergaard M, Hansen AJ. Spreading depression is not associated with neuronal injury in the normal brain. Brain Res. 1988; 449:395–398. [PubMed: 3395856]
16. Kraig RP, Mitchell HM, Christie-Pope B, et al. TNF-alpha and Microglial Hormetic Involvement in Neurological Health & Migraine. Dose Response. 2010; 8:389–413. [PubMed: 21191481]
17. Pusic AD, Kraig RP. Inflammatory gene micro array profiling demonstrates “T-cell-like” activation after recurrent spreading depression - implications for migraine pathogenesis. Soc Neurosci. 2010; 36 Prog #346.2.
18. Pusic AD, Mitchell HM, Kraig RP. IFN-γ from T-cells modulates susceptibility to- and transient demyelination from - spreading depression: implications for migraine therapy. Soc Neurosci. 2011; 37 Prog #875.16.
19. Bures, J.; Buresova, O.; Krivanek, J. The Mechanism and Applications of Leao’s Spreading Depression of Electroencephalographic Activity. Prague: Academia; 1974.
20. Somjen GG. Mechanisms of spreading depression and hypoxic spreading depressionlike depolarization. Physiol Rev. 2001; 81:1065–1096. [PubMed: 11427692]
21. Kovacs R, Papageorgiou I, Heinemann U. Slice cultures as a model to study neurovascular coupling and blood brain barrier *in vitro* . Cardiovasc Psychiatry Neurol. 2011:646958. [PubMed: 21350722]
22. Hulse RE, Swenson WG, Kunkler PE, White DM, Kraig RP. Monomeric IgG is neuroprotective via enhancing microglial recycling endocytosis and TNF-alpha. J Neurosci. 2008; 28:12199–12211. [PubMed: 19020014]
23. Kraig RP, Dong LM, Thisted R, Jaeger CB. Spreading depression increases immunohistochemical staining of glial fibrillary acidic protein. J Neurosci. 1991; 11:2187–2198. [PubMed: 1906091]
24. Grinberg YY, Milton JG, Kraig RP. Spreading depression sends microglia on Levy flights. PLoS One. 2011; 6:e19294. [PubMed: 21541289]
25. Ransohoff RM, Perry VH. Microglial physiology: unique stimuli, specialized responses. Annu Rev Immunol. 2009; 27:119–145. [PubMed: 19302036]
26. Gehrmann J, Mies G, Bonnekoh P, Banati R, Iijima T, Kreutzberg GW, Hossmann KA. Microglial reaction in the rat cerebral cortex induced by cortical spreading depression. Brain Pathol. 1993; 1:11–17. [PubMed: 8269080]
27. Caggiano AO, Kraig RP. Eicosanoids and nitric oxide influence induction of reactive gliosis from spreading depression in microglia but not astrocytes. J Comp Neurol. 1996; 369:93–108. [PubMed: 8723705]
28. Pusic KM, Pusic AD, Kemme J, Kraig RP. Spreading depression requires microglia and is decreased by their M2a polarization from environmental enrichment. Glia. 2014; 62:1176–1194. [PubMed: 24723305]
29. Grinberg YY, Kraig RP. Intranasal delivery of IGF-1 decreases spreading depression susceptibility in rat. Soc. Neurosci. 2013; 39 Prog: #822.06.
30. Pusic AD, Kraig RP. Youth and environmental enrichment generate serum exosomes containing miR-219 that promote CNS myelination. Glia. 2014; 62:284–299. [PubMed: 24339157]
31. Pusic AD, Pusic KM, Clayton BL, Kraig RP. IFNgamma-stimulated dendritic cell exosomes as a potential therapeutic for remyelination. J Neuroimmunol. 2014; 266:12–23. [PubMed: 24275061]
32. Pusic AD, Grinberg YY, Mitchell HM, Kraig RP. Modeling neural immune signaling of episodic and chronic migraine using spreading depression in vitro. J Vis Exp. (52) pii: 2910.
33. Kunkler PE, Kraig RP. Reactive astrocytosis from excitotoxic injury in hippocampal organ culture parallels that seen in vivo. J Cereb Blood Flow Metab. 1997; 17:26–43. [PubMed: 8978384]
34. Pomper JK, Haack S, Petzold GC, Buchheim K, Gabriel S, Hoffman U, Heinemann U. Repetitive spreading depression-like events result in cell damage in juvenile hippocampal slice cultures maintained in normoxia. J Neurophysiol. 2006; 95:355–368. [PubMed: 16177179]
35. Dreier JP, Major S, Pannek HW, Woitzik J, Scheel M, Wiesenthal D, Martus P, Winkler MKL, Hartings JA, Fabricius M, Speckmann EJ, Gorji A. COSBID study group. Spreading convulsions,

spreading depolarizations and epileptogenesis in human cerebral cortex. Brain. 2011; 135:259–275. [PubMed: 22120143]

36. Palmer JE, Chronicle EP, Rolan P, Mulleners WM. Cortical hyperexcitability is cortical under-inhibition: evidence from a novel functional test of migraine patients. Cephalalgia. 2000; 20:525–532. [PubMed: 11075834]
37. Mulleners WM, Chronicle EP, Palmer JE, Koehler PJ, Vredeveld JW. Visual cortex excitability in migraine with and without aura. Headache. 2001; 41:565–572. [PubMed: 11437892]
38. Welch KM. Brain hyperexcitability: the basis for antiepileptic drugs in migraine prevention. Headache. 2005; 45:S25–S32. [PubMed: 15833087] Suppl 1
39. Brennan KC. Turn down the lights!: an irritable occipital cortex in migraine without aura. Neurology. 2011; 76:206–207. [PubMed: 21148117]
40. Mathew PG, Mathew T. Taking care of the challenging tension headache patient. Curr Pain Headache Rep. 2011; 15:444–450. [PubMed: 21845469]
41. Calabrese EJ, Bachmann KA, Bailer AJ, et al. Biological stress response terminology: Integrating the concepts of adaptive response and preconditioning stress within a hormetic dose-response framework. Toxicol Appl Pharmacol. 2007; 222:122–128. [PubMed: 17459441]
42. Wheeler D, Knapp E, Bandaru VV, et al. Tumor necrosis factor-alpha-induced neutral sphingomyelinase-2 modulates synaptic plasticity by controlling the membrane insertion of NMDA receptors. J Neurochem. 2009; 109:1237–1249. [PubMed: 19476542]
43. Mitchell HM, White DM, Kraig RP. Strategies for study of neuroprotection from cold-preconditioning. J Vis Exp. (43) pii: 2192.
44. Mitchell HM, White DM, Domowicz MS, Kraig RP. Cold pre-conditioning neuroprotection depends on TNF-alpha and is enhanced by blockade of interleukin-11. J Neurochem. 2011; 117:187–196. [PubMed: 21070241]
45. Pfaffl MW. A new mathematical model for relative quantification in real-time RT-PCR. Nucleic Acids Res. 2001; 29:e45. [PubMed: 11328886]
46. Caggiano AO, Breder CD, Kraig RP. Long-term elevation of cyclooxygenase-2, but not lipoxygenase, in regions synaptically distant from spreading depression. J Comp Neurol. 1996; 376:447–462. [PubMed: 8956110]
47. Dickinson DA, Forman HJ. Glutathione in defense and signaling: lessons from a small thiol. Ann N Y Acad Sci. 2002; 973:488–504. [PubMed: 12485918]
48. Kraig RP, Dong LM, Thisted R, Jaeger CB. Spreading depression increases immunohistochemical staining of glial fibrillary acidic protein. J Neurosci. 1991; 11:2187–2198. [PubMed: 1906091]
49. Kunkler PE, Kraig RP. Hippocampal spreading depression bilaterally activates the caudal trigeminal nucleus in rodents. Hippocampus. 2003; 13:835–844. [PubMed: 14620879]
50. Kreutzberg GW. Microglia, the first line of defence in brain pathologies. Arzneimittelforschung. 1995; 45:357–360. [PubMed: 7763326]
51. Tamura Y, Eguchi A, Jin G, Sami MM, Kataoka Y. Cortical spreading depression shifts cell fate determination of progenitor cells in the adult cortex. J Cereb Blood Flow Metab. 2012; 32:1879–1887. [PubMed: 22781335]
52. Saida T, Saida K, Silberberg DH. Demyelination produced by experimental allergic neuritis serum and anti-galactocerebroside antiserum in CNS cultures. Acta Neuropathol. 1979; 48:19–25. 42. [PubMed: 506686]
53. Dal Canto MC, Lipton HL. Primary demyelination in Theiler's virus infection. An ultrastructural study. Lab Invest. 1975; 33:626–637. [PubMed: 1202282]
54. Lucchinetti CF, Popescu BF, Bunyan RF, et al. Inflammatory cortical demyelination in early multiple sclerosis. N Engl J Med. 2011; 365:2188–2197. [PubMed: 22150037]
55. Oppenheim, JJ.; Feldmann, M. Introduction to the role of cytokines in innate host defense and adaptive immunity. In: Oppenheim, JJ.; Feldmann, M., editors. Cytokine reference : a compendium of cytokines and other mediators of host defense. Vol. 1. Ligands. San Diego: Academic Press; 2001. p. 3-20.
56. MacIlwain, H.; Bachelard, HS. Biochemistry and the central nervous system. Edinburgh: Churchill Livingstone; 1971.

57. Muller M, Fontana A, Zbinden G, Gahwiler BH. Effects of interferons and hydrogen peroxide on CA3 pyramidal cells in rat hippocampal slice cultures. Brain Res. 1993; 619:157–162. [PubMed: 8374773]
58. Renno T, Krakowski M, Piccirillo C, Lin JY, Owens T. TNF-alpha expression by resident microglia and infiltrating leukocytes in the central nervous system of mice with experimental allergic encephalomyelitis. Regulation by Th1 cytokines. J Immunol. 1995; 154:944–953. [PubMed: 7814894]
59. Vollmer TL, Waldor MK, Steinman L, Conley FK. Depletion of T-4+ lymphocytes with monoclonal antibody reactivates toxoplasmosis in the central nervous system: a model of superinfection in AIDS. J Immunol. 1987; 138:3737–3741. [PubMed: 3108372]
60. Chakraborty G, Ziemba S, Drivas A, Ledeen RW. Myelin contains neutral sphingomyelinase activity that is stimulated by tumor necrosis factor-alpha. J Neurosci Res. 1997; 50:466–476. [PubMed: 9364332]
61. Luberto C, Hassler DF, Signorelli P, et al. Inhibition of tumor necrosis factor-induced cell death in MCF7 by a novel inhibitor of neutral sphingomyelinase. J Biol Chem. 2002; 277:41128–41139. [PubMed: 12154098]
62. Silverberg J, Ginsburg D, Orman R, Amassian V, Durkin HG, Stewart M. Lymphocyte infiltration of neocortex and hippocampus after a single brief seizure in mice. Brain Behav Immun. 2010; 24:263–272. [PubMed: 19822204]
63. Ye Y, Xiong J, Hu J, et al. Altered hippocampal myelinated fiber integrity in a lithium-pilocarpine model of temporal lobe epilepsy: a histopathological and stereological investigation. Brain Res. 2013; 1522:76–87. [PubMed: 23727401]
64. Watanabe S, Matsuo H, Kobayashi Y, et al. Transient degradation of myelin basic protein in the rat hippocampus following acute carbon monoxide poisoning. Neurosci Res. 2010; 68:232–240. [PubMed: 20633582]
65. Liu MC, Akle V, Zheng W, et al. Extensive degradation of myelin basic protein isoforms by calpain following traumatic brain injury. J Neurochem. 2006; 98:700–712. [PubMed: 16893416]
66. Blakemore WF, Keirstead HS. The origin of remyelinating cells in the central nervous system. J Neuroimmunol. 1999; 98:69–76. [PubMed: 10426364]
67. McTigue DM, Wei P, Stokes BT. Proliferation of NG2-positive cells and altered oligodendrocyte numbers in the contused rat spinal cord. J Neurosci. 2001; 21:3392–3400. [PubMed: 11331369]
68. McIver SR, Muccigrosso M, Gonzales ER, et al. Oligodendrocyte degeneration and recovery after focal cerebral ischemia. Neuroscience. 2010; 169:1364–1375. [PubMed: 20621643]
69. Wadman WJ, Juta AJ, Kamphuis W, Somjen GG. Current source density of sustained potential shifts associated with electrographic seizures and with spreading depression in rat hippocampus. Brain Res. 1992; 570:85–91. [PubMed: 1617432]
70. Kunkler PE, Hulse RE, Schmitt MW, Nicholson C, Kraig RP. Optical current source density analysis in hippocampal organotypic culture shows that spreading depression occurs with uniquely reversing currents. J Neurosci. 2005; 25:3952–3961. [PubMed: 15829647]
71. Martens-Mantai T, Speckmann EJ, Gorji A. Propagation of cortical spreading depression into the hippocampus: The role of the entorhinal cortex. Synapse. 2014
72. Eikermann-Haerter K, Yuzawa I, Qin T, et al. Enhanced subcortical spreading depression in familial hemiplegic migraine type 1 mutant mice. J Neurosci. 2011; 31:5755–5763. [PubMed: 21490217]
73. Fifkova E, Bures J. Spreading depression in the mammalian striatum. Arch Int Physiol Biochim. 1964; 72:171–179. [PubMed: 4157763]
74. Vinogradova LV, Koroleva VI, Bures J. Re-entry waves of Leao's spreading depression between neocortex and caudate nucleus. Brain Res. 1991; 538:161–164. [PubMed: 2018928]
75. Bek S, Genc G, Demirkaya S, Eroglu E, Odabasi Z. Ophthalmoplegic migraine. Neurologist. 2009; 15:147–149. [PubMed: 19430270]
76. Mark AS, Blake P, Atlas SW, Ross M, Brown D, Kolsky M. Gd-DTPA enhancement of the cisternal portion of the oculomotor nerve on MR imaging. AJNR Am J Neuroradiol. 1992; 13:1463–1470. [PubMed: 1414843]

77. Stommel EW, Ward TN, Harris RD. MRI findings in a case of ophthalmoplegic migraine. Headache. 1993; 33:234–237. [PubMed: 8320096]

78. Mark AS, Casselman J, Brown D, et al. Ophthalmoplegic migraine: reversible enhancement and thickening of the cisternal segment of the oculomotor nerve on contrast-enhanced MR images. AJNR Am J Neuroradiol. 1998; 19:1887–1891. [PubMed: 9874541]

79. Romano LM, Besocke AG. Teaching video neuroimages: recurrent oculomotor neuropathy with isolated ptosis vs ophthalmoplegic migraine. Neurology. 2009; 72:e44. [PubMed: 19255404]

80. Manack AN, Buse DC, Lipton RB. Chronic migraine: epidemiology and disease burden. Curr Pain Headache Rep. 2011; 15:70–78. [PubMed: 21063918]

81. Haut SR, Bigal ME, Lipton RB. Chronic disorders with episodic manifestations: focus on epilepsy and migraine. Lancet Neurol. 2006; 5:148–157. [PubMed: 16426991]

82. Bigal ME, Lipton RB. Migraine chronification. Curr Neurol Neurosci Rep. 2011; 11:139–148. [PubMed: 21243447]

83. Silberstein, SD.; Olesen, J. Chronic migraines. In: Olesen, J.; Goadsby, P.; Ramadan, N.; Tfelt-Hansen, A.; Welch, KMA., editors. The Headaches. 3rd ed.. Philadelphia: Lippincott-Raven; 2005. p. 613-617.

84. Lambert GA, Zagami AS. The mode of action of migraine triggers: a hypothesis. Headache. 2009; 49:253–275. [PubMed: 18793210]

85. Mulleners WM, Chronicle EP, Vredeveld JW, Koehler PJ. Cortical excitability in migraine. Ann Neurol. 1999; 45:415–416. [PubMed: 10072064]

86. Pietrobon D, Striessnig J. Neurobiology of migraine. Nat Rev Neurosci. 2003; 4:386–398. [PubMed: 12728266]

87. Custers A, Mulleners WM, Chronicle EP. Assessing cortical excitability in migraine: reliability of magnetic suppression of perceptual accuracy technique over time. Headache. 2005; 45:1202–1207. [PubMed: 16178950]

88. Pietrobon D. Migraine: new molecular mechanisms. Neuroscientist. 2005; 11:373–386. [PubMed: 16061523]

89. van den Maagdenberg AM, Pietrobon D, Pizzorusso T, et al. A Cacna1a knockin migraine mouse model with increased susceptibility to cortical spreading depression. Neuron. 2004; 41:701–710. [PubMed: 15003170]

90. Kager H, Wadman WJ, Somjen GG. Simulated seizures and spreading depression in a neuron model incorporating interstitial space and ion concentrations. J Neurophysiol. 2000; 84:495–512. [PubMed: 10899222]

91. Liebetanz D, Fregni F, Monte-Silva KK, et al. After-effects of transcranial direct current stimulation (tDCS) on cortical spreading depression. Neurosci Lett. 2006; 398:85–90. [PubMed: 16448754]

92. Pietrobon D, Moskowitz MA. Chaos and commotion in the wake of cortical spreading depression and spreading depolarizations. Nat Rev Neurosci. 2014; 15:379–393. [PubMed: 24857965]

93. Denuelle M, Boulloche N, Payoux P, Fabre N, Trotter Y, Geraud G. A PET study of photophobia during spontaneous migraine attacks. Neurology. 2011; 76:213–218. [PubMed: 21148120]

94. Aurora SK, Ahmad BK, Welch KM, Bhardhwaj P, Ramadan NM. Transcranial magnetic stimulation confirms hyperexcitability of occipital cortex in migraine. Neurology. 1998; 50:1111–1114. [PubMed: 9566403]

95. Woods RP, Iacoboni M, Mazziotta JC. Brief report: bilateral spreading cerebral hypoperfusion during spontaneous migraine headache. N Engl J Med. 1994; 331:1689–1692. [PubMed: 7969360]

96. Cao Y, Welch KM, Aurora S, Vikingstad EM. Functional MRI-BOLD of visually triggered headache in patients with migraine. Arch Neurol. 1999; 56:548–454. [PubMed: 10328249]

97. Launer LJ, Terwindt GM, Ferrari MD. The prevalence and characteristics of migraine in a population-based cohort: the GEM study. Neurology. 1999; 53:537–542. [PubMed: 10449117]

98. Hoffmann K, Lindner M, Groticke I, Stangel M, Loscher W. Epileptic seizures and hippocampal damage after cuprizone-induced demyelination in C57BL/6 mice. Exp Neurol. 2008; 210:308–321. [PubMed: 18096162]

99. Empl M, Sostak P, Breckner M, et al. T-cell subsets and expression of integrins in peripheral blood of patients with migraine. Cephalalgia. 1999; 19:713–707. discussion 697. [PubMed: 10570725]
100. Renno T, Krakowski M, Piccirillo C, et al. TNF-α expression by resident microglia and inflitrating leukocytes in the central nervous system of mice with experimental allergic encephalomyelitis. J Immunol. 1995; 15:944–953. [PubMed: 7814894]
101. Mir M, Asensio VJ, Tolosa L, et al. Tumor necrosis factor alpha and interferon gamma cooperatively induce oxidative stress and motoneuron death in rat spinal cord embryonic explants. Neuroscience. 2009; 162:959–971. [PubMed: 19477238]
102. Kuzina ES, Chernolovskaya EL, Kudriaeva AA, et al. Immunoproteasome enhances intracellular proteolysis of myelin basic protein. Dokl Biochem Biophys. 2013; 453:300–303. [PubMed: 24385101]
103. Tuncel D, Tolun FI, Gokce M, Imrek S, Ekerbicer H. Oxidative stress in migraine with and without aura. Biol Trace Elem Res. 2008; 126:92–97. [PubMed: 18690416]
104. Liu B, Andrieu-Abadie N, Levade T, Zhang P, Obeid LM, Hannun YA. Glutathione regulation of neutral sphingomyelinase in tumor necrosis factor-alpha-induced cell death. J Biol Chem. 1998; 273:11313–11320. [PubMed: 9556624]
105. Jana A, Pahan K. Oxidative stress kills human primary oligodendrocytes via neutral sphingomyelinase: implications for multiple sclerosis. J Neuroimmune Pharmacol. 2007; 2:184–193. [PubMed: 18040843]
106. Rutkute K, Asmis RH, Nikolova-Karakashian MN. Regulation of neutral sphingomyelinase-2 by GSH: a new insight to the role of oxidative stress in aging-associated inflammation. J Lipid Res. 2007; 48:2443–2452. [PubMed: 17693623]
107. Filosto S, Ashfaq M, Chung S, Fry W, Goldkorn T. Neutral sphingomyelinase 2 activity and protein stability are modulated by phosphorylation of five conserved serines. J Biol Chem. 2012; 287:514–522. [PubMed: 22074919]
108. Jana A, Pahan K. Sphingolipids in multiple sclerosis. Neuromolecular Med. 2010; 12:351–361. [PubMed: 20607622]
109. Lee DW, Banquy X, Kristiansen K, Kaufman Y, Boggs JM, Israelachvili JN. Lipid domains control myelin basic protein adsorption and membrane interactions between model myelin lipid bilayers. Proc Natl Acad Sci U S A. 2014; 111:E768–E775. [PubMed: 24516125]
110. Musse AA, Harauz G. Molecular “negativity” may underlie multiple sclerosis: role of the myelin basic protein family in the pathogenesis of MS. Int Rev Neurobiol. 2007; 79:149–172. [PubMed: 17531841]
111. Nave KA. Neurological mouse mutants and the genes of myelin. J Neurosci Res. 1994; 38:607–612. [PubMed: 7807578]
112. Zhao YY, Shi XY, Qiu X, et al. Enriched environment increases the myelinated nerve fibers of aged rat corpus callosum. Anat Rec (Hoboken). 2012; 295:999–1005. [PubMed: 22431229]

HIGHLIGHTS

- Multiple sclerosis and migraine with aura show highly correlated myelin abnormalities
- Spreading depression, the cause of migraine with aura, transiently disrupts myelin
- Myelin disruption may promote spreading depression by enhancing aberrant excitability
- Interferon-gamma from T cells increases oxidative stress from spreading depression
- In turn, oxidative stress activates sphingomyerlinase-2, resulting in myelin disruption

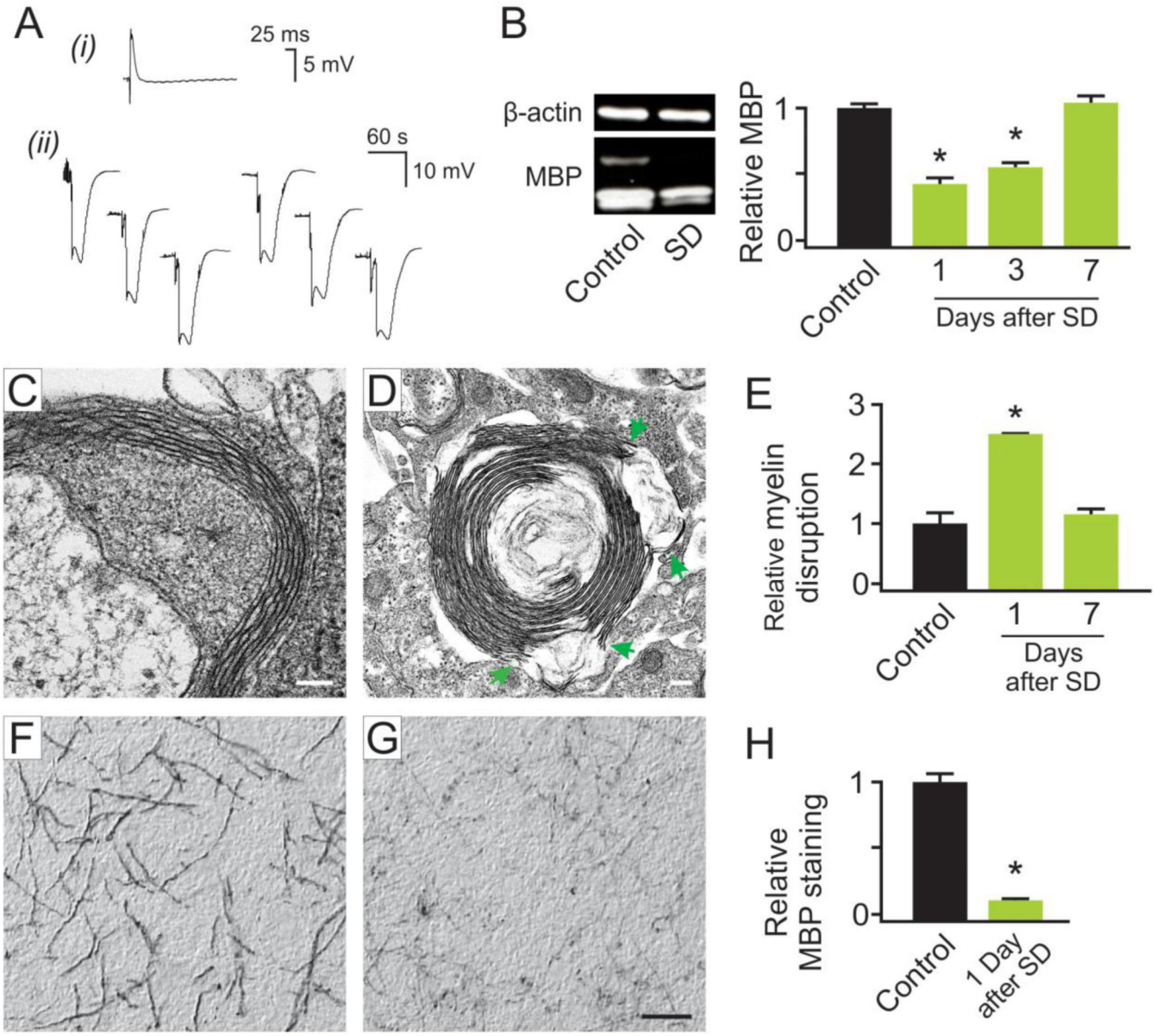

Figure 1. Recurrent spreading depression transiently disrupted myelin and reduced myelin basic protein in slice cultures

Representative electrophysiological records **(A)** of spreading depression (SD) are shown, with a representative field potential *(i)* confirming slice synaptic vitality, of the slice, and representative recording of six SDs *(ii)*. Western blot analyses for myelin basic protein (MBP). **(B)** show a transient and significant (*$p < 0.001$) reduction in myelin one day after SD, which progressively returned to control levels. Electron microscopy images were derived from the CA3 hippocampal slice culture area. Control images **(C)** showed little evidence of myelin sheath disruption. However, SD triggered a significant (*$p < 0.001$) increase in myelin disruption after one day with blebs (arrows) between myelin layers **(D)** which returned to control levels by seven days. Scale bars, 100 nm (C), and 200 nm (D). Cells with myelin disruptions were quantified per image **(E)**, and revealed a significant

difference in myelin breakage at one day post SD, which returned to control levels by seven days post SD. Representative images of MBP immuno-staining from control **(F)** and one day after SD **(G)** likewise show a reduction in MBP. Densitometric quantification of immunostaining **(H)** confirmed a significant (**p* = 0.01) reduction of MBP one day after SD. Scale bar, 50 μm. Numerical data are mean ± SEM and comparisons between groups made via ANOVA plus Holm-Sidak *post hoc* testing (B and E) and paired Student's *t*-test (H).

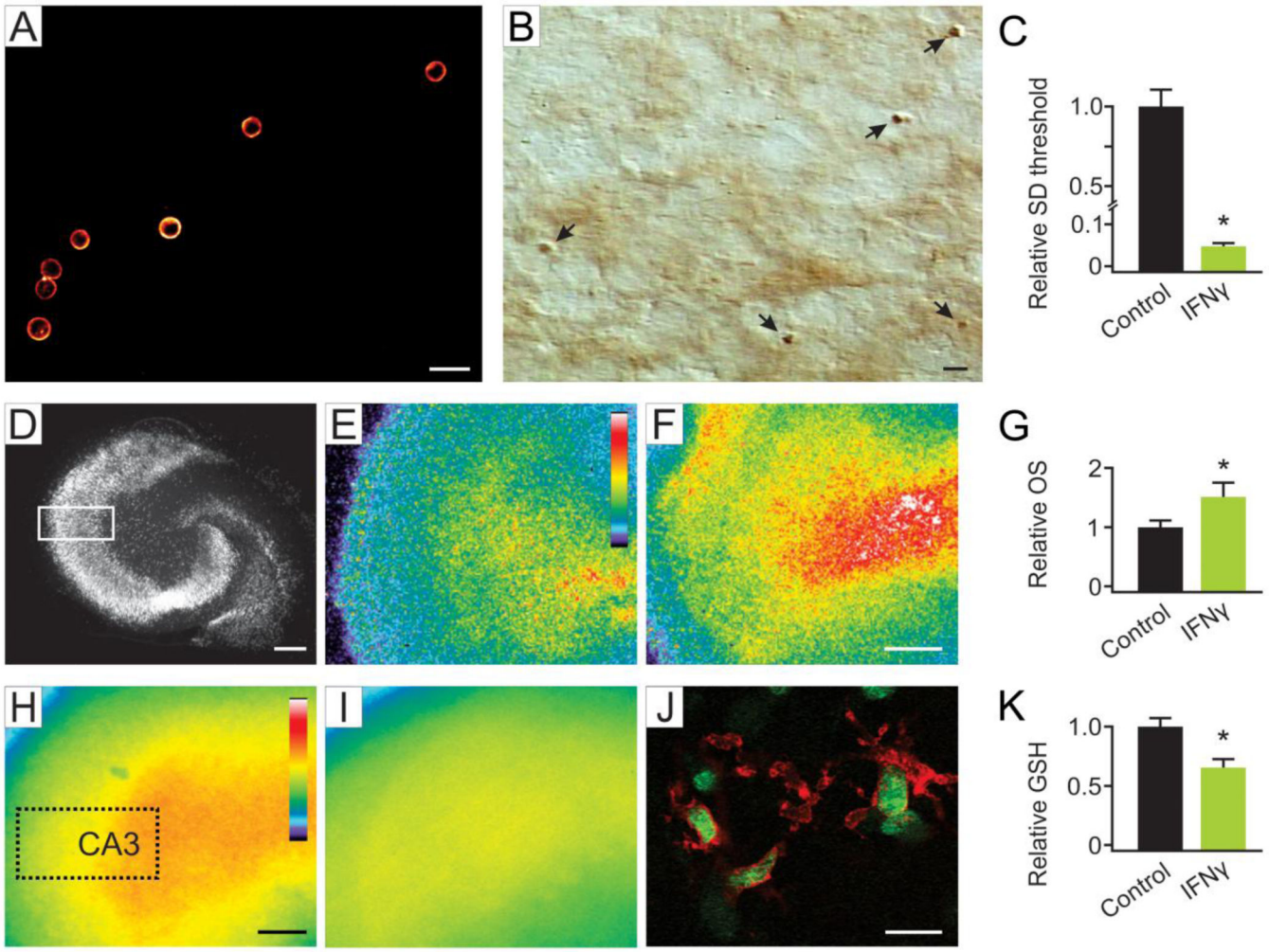

Figure 2. T cells in slice cultures produced IFNγ which acutely reduced spreading depression threshold

Confocal fluorescence image showing immunostaining of T cells **(A)** in parenchyma of hippocampal slice cultures with CD6, a pan T cell marker. Scale bar, 15 μm. Lipopolysaccharide stimulation of cultures significantly (*p = 0.002) increased the number of IFNγ positive cells (bright field image of diaminobenzidine-positive cells) that morphologically resembled T cells compared to untreated cultures. Representative image **(B)** shows IFNγ positive cells (arrows). Scale bar, 30 μm. Acute application of IFNγ at a non-toxic dose caused a significant (*p < 0.001) reduction in SD threshold **(C)**. Oxidative stress (OS) induced by acute exposure to IFNγ was measured via CellROX, a fluorescent marker of OS. NeuN immunostained image **(D)** illustrates the area of interest (dotted line) used for quantification. Scale bar, 200 μm. Lower levels of OS are evident in control **(E)** compared to IFNγ treated slice cultures **(F)**. Scale bar, 200 μm. Quantification of fluorescence intensity **(G)** shows that acute IFNγ exposure triggered a significant (*p < 0.001) increase in OS. Intracellular glutathione (GSH) was visualized using ThiolTracker, a fluorescent probe that reacts strongly with thiols. Representative low-power images show regional GSH under control conditions **(H)** and 30 minutes after treatment with IFNγ **(I)**.

Scale bar, 200 μm. Representative high-power confocal image **(J)** shows ThiolTracker staining (arrows; green) within microglia (arrow heads; red). Scale bar, 20 μm. Quantification of regional staining intensity **(K)** revealed a significant (**p* = 0.007) decrease in GSH content following acute IFNγ exposure. Numerical data are mean ± SEM and comparisons between groups made via ANOVA plus Holm-Sidak *post hoc* testing.

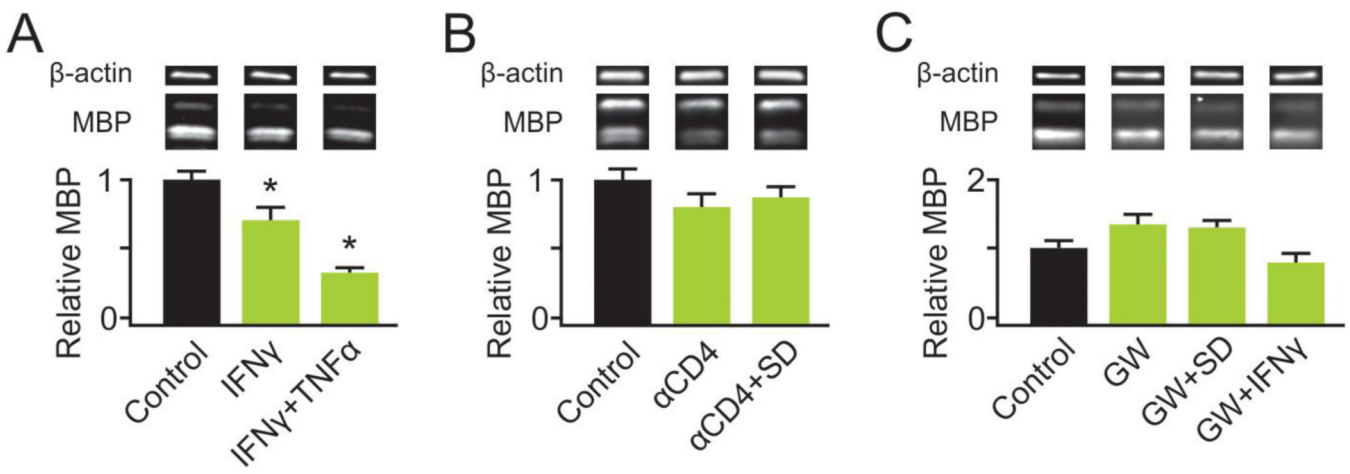

Figure 3. T cells/IFNγ and sphingomyelinase activity are responsible for loss of myelin basic protein following spreading depression

Western blot analysis of MBP was used to determine changes in myelin following various treatments of slice cultures. IFNγ exposure triggered a significant (*$p = 0.04$) decline in MBP, a loss that was significantly enhanced (*$p < 0.001$) by co-incubation with TNFα (100 ng/mL) **(A)**. Removal of T cells from slice cultures at seven days *in vitro* by exposure to anti-CD4 (αCD4) did not alter MBP levels when measured at 21 or more days *in vitro* **(B)**. However, removal of T cells abrogated the decrease in MBP seen one day after SD. Pharmacological inhibition of neutral sphingomyelinase-2 by GW4869 prevented the loss of MBP otherwise seen one day after SD or exposure to IFNγ **(C)**. Numerical data are mean ± SEM and comparisons between groups made via ANOVA plus Holm-Sidak *p ost hoc* testing.

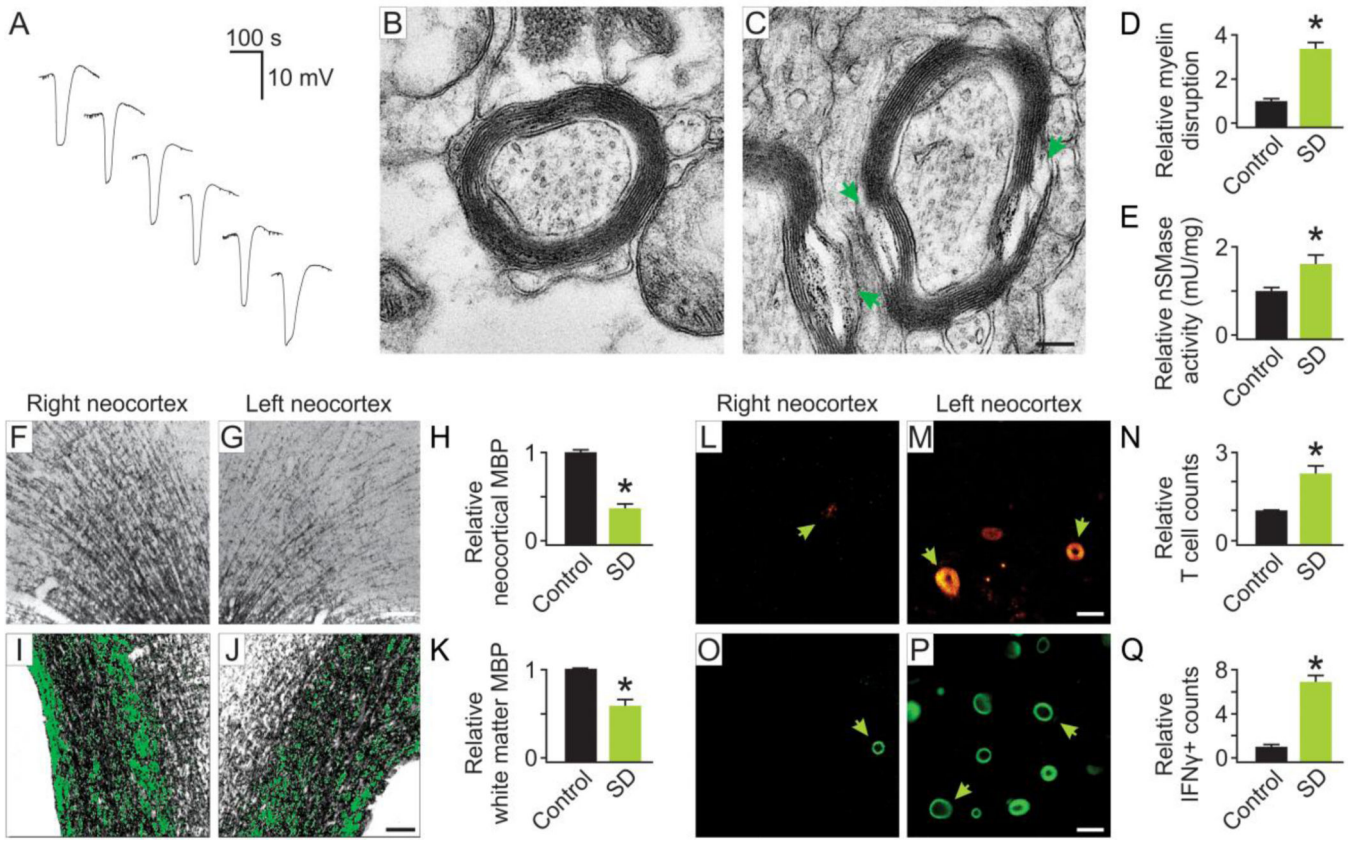

Figure 4. ***In vivo*** **spreading depression recapitulated** ***in vitro*** **results**

Representative electrophysiological records **(A)** are shown for KCl-induced whole animal neocortical recurrent spreading depression (SD). All subsequent measurements were taken one day post exposure to SD. Representative electron microscopy images were derived from the paramedian neocortex. While control images **(B)** showed little evidence of damage to the myelin sheath, exposure to SD **(C)** caused significant (**p* = 0.001) structural disruption (arrows) of myelin one day later **(D)**. Scale bar, 200 nM. Neutral sphingomyelinase activity (mU/mg protein normalized to control, with U defined as the amount of nSMase2 that will catalyze transformation of one micromole of sphingomyelin per minute) was significantly (**p* = 0.02) increased in SD-exposed neocortex (left) compared to the contralateral control neocortex (right) **(E)**. Comparison of MBP staining control **(F)** versus SD-exposed neocortex **(G)** revealed a significant (**p* < 0.001) reduction in grey matter myelin following SD **(H)**. Scale bar, 100 μm. A significant (**p* < 0.001) decrease in MBP immunostaining following SD was also seen in the underlying white matter of the lateral corpus callosum **(I–K)**. Thresholded areas are shaded green to aid visualization of differences that were densitometrically quantified (**p* < 0.001). Scale bar, 100 μm. Representative confocal fluorescence images show immunostaining of T cells (arrows) within neocortex of control **(L)** and SD-exposed **(M)** brain. Scale bar, 30 μm. Quantification **(N)** shows significantly (**p* < 0.001) increased T cell counts in SD versus control neocortex. Representative images show IFNγ positive cells that morphologically resemble T cells (arrows) in control **(O)** and SD-exposed neocortex **(P)**. Scale bar, 30 μm. Quantification revealed a significant (**p*

<0.001) increase in IFNγ-positive cells following exposure to SD **(Q)**. Numerical data are mean ± SEM and comparisons between groups made via Student's t-Test.

Table 1
Slice culture T cell lymphocyte-related mRNA changes after spreading depression

Slice culture expression of inflammatory and common cytokines following exposure to SD was assayed via PCR arrays. Relative gene expression was normalized to ribosomal protein L13a (Rpl13a). Greater than two-fold changes in expression between SD and control conditions were considered significant.[43–45] mRNA analyses included two technical replicates per experimental measurement and at least three biological replicates per experimental group. Table 1 lists changes in T cell-related mRNA species measured three hours after induction of six SDs. For assaying subtle changes in IFNγ expression, cDNA for both experimental and control samples were pre-amplified. Red numbers indicate a significant decrease, and green numbers indicate a significant increase in expression.

Rat Slice Culture Post-SD vs. Control			
Cytokine mRNA changes			
Symbol	**Ref Seq**	**Description**	**Fold Regulation**
T cell lymphocytes			
IFNγ	NM_138880	Interferon-gamma	4.66 (preamp)
Csf1	NM_023981	Colony stimulating factor 1	2.46
Csf2	XM_340799	Colony stimulating factor 2	4.0
IL-2	NM_053836	Interleukin 2	4.2
IL-3	NM_031513	Interleukin 3	4.4
IL-21	XM_345201	Interleukin 21	11.0
Neuron			
IL-11	NM_133519	Interleukin 11	5.46
Bmp2	NM_017178	Bone morphogenetic protein 2	2.6
IL-1ra	NM_022194	Interleukin 1 receptor antagonist	9.19
Microglia			
TNFα	NM_012675	Tumor necrosis factor-alpha	8.88
IL-6	NM_012589	Interleukin 6	3.4
IL-12a	NM_053390	Interleukin 12a	4.0
IL-19	XM_001060482	Interleukin 19	6.1
IL-10	NM_012854	Interleukin 10	2.23
Astrocytes			
IL-1α	NM_017019	Interleukin 1 alpha	3.36
IL-1β	NM_031512	Interleukin 1 beta	9.51
Lif	NM_022196	Leukemia inhibitory factor	17.15